Inorg. Chem. **2008**, *47*, 951–956

Ruthenium(II) 2,2′-Bipyridyl Tetrakis Acetonitrile Undergoes Selective Axial Photocleavage

Agustín Petroni, Leonardo D. Slep, and Roberto Etchenique*

Departamento de Química Inorgánica, Analítica y Química Física, INQUIMAE, Facultad de Ciencias Exactas y Naturales Universidad de Buenos Aires, Pabellón 2, Ciudad Universitaria, C1428EHA Buenos Aires, Argentina

Received September 14, 2007

The complex $[Ru(bpy)(AN)_4]^{2+}$ (bpy = 2,2′-bipyridyl, AN = acetonitrile) has a Ru(II) $\rightarrow \pi^*_{bpy}$ MLCT band at 388 nm. Upon irradiation on this absorption band, the compound undergoes total regioselective photocleavage yielding complexes *fac*-$[Ru(bpy)(AN)_3(H_2O)]^{2+}$ and *trans*-$[Ru(bpy)(AN)_2(H_2O)_2]^{2+}$ in two consecutive steps with quantum yields of 0.43 and 0.09, respectively. This behavior is a consequence of the stronger σ-donor ability of the bpy nitrogens that determines the orbital ordering and therefore the nature of the lowest lying ^{3}d–d state responsible for the photochemistry. The two-step photoreaction, which can be followed by UV–vis and NMR spectra, provides a quantitative path to the preparation of *trans*-polypyridine species with potentially interesting photochemical properties.

Introduction

The photochemistry of ruthenium polypyridyl complexes has been extensively studied. Irradiation of a strong Ru(II) $\rightarrow \pi^*_{bpy}$ MLCT band located usually in the visible range of the spectrum allows for the thermal population of a nearby ^{3}d−d dissociative state with sufficiently long lifetime to undergo photochemical reactions that yield free ligand molecules and a ruthenium polypyridyl residue, generally an aquo or solvento complex.[1−4] Even ruthenium(II) tris-bipyridine $[Ru(bpy)_3]^{2+}$ (bpy = 2,2′-bipyridine), perhaps the most frequently employed Ru(II) polypyridine compound, though usually stable upon irradiation, has been reported as being capable of clean photochemistry in nonaqueous solutions containing halides or pseudohalides, yielding the well-characterized *cis*-$Ru(bpy)_2X_2$ species.[5,6] In the series of $[Ru(bpy)_2L_2]^{n+}$ (L = any ligand) compounds, the photodissociation process usually involves the monodentate L ligand and has been employed both in heteroleptic syntheses[7] and in biomolecule photodelivery in which the metal moiety acts as a cage for visible light phototriggering.[8−10]

The photochemistry of Ru(II) complexes bearing only one bipyridine fragment and four non-bipyridine ligands, usually employed as intermediates in the synthesis of heteroleptic polipyridine compounds,[11,12] has not been sufficiently explored. This is surprising since simpler structures are expected to yield photochemical processes that should be easier to understand and rationalize. We focus on the photoreactivity of $[Ru(bpy)(AN)_4]^{2+}$ (AN = CH_3CN), a species which has been well known for more than 30 years. Schrock et al. early demonstrated that the thermal substitution in $[Ru(bpy)_2(AN)_4]BF_4$ occurs solely on the equatorial ligands.[11] In contrast, we report here that $[Ru(bpy)AN_4]^{2+}$ undergoes clean photochemistry upon irradiation with visible light that leads to substitution of axial ligands, yielding *fac*-$[Ru(bpy)(AN)_3(H_2O)]^{2+}$ and *trans*-$[Ru(bpy)(AN)_2(H_2O)_2]^{2+}$ in two consecutive steps. This complex is therefore a valuable

* To whom correspondence should be addressed. E-mail: rober@qi.fcen.uba.ar.

(1) Pinnick, D. V.; Durham, B. *Inorg. Chem.* **1984**, *23*, 1440.
(2) Pinnick, D. V.; Durham, B. *Inorg. Chem.* **1984**, *23*, 3842.
(3) Durham, B.; Wilson, S. R.; Hodgson, D. J.; Meyer, T. J. *J. Am. Chem. Soc.* **1980**, *102* (2), 600.
(4) Collin, J. P.; Jouvenot D.; Koizumi, M.; Sauvage, J. P. *Inorg. Chem.* **2005**, *44* (13), 4693.
(5) Wallace, W. M.; Hoggard, P. E. *Inorg. Chem.* **1979**, *18* (10), 2934.
(6) Durham, B.; Caspar, J. V.; Nagle, J. K.; Meyer, T. J. *J. Am. Chem. Soc.* **1982**, *104*, 4803.
(7) Durham, B.; Walsh, J. L.; Carter, C. L.; Meyer, T. J. *Inorg. Chem.* **1980**, *19*, 860.
(8) Zayat, L.; Calero, C.; Alborés, P.; Baraldo, L.; Etchenique, R. *J. Am. Chem. Soc.* **2003**, *125*, 882.
(9) Nikolenko, V.; Yuste, R.; Zayat, L.; Baraldo, L. M.; Etchenique, R. *Chem. Commun.* **2005**, 1752.
(10) Zayat, L.; Salierno, M.; Etchenique, R. *Inorg. Chem.* **2006**, *45*, 1728.
(11) Schrock, R. R.; Johnson, B. F .G.; Lewis, J. *J. Chem. Soc., Dalton* **1974**, 951.
(12) Freedman, D. A.; Kruger, S.; Roosa, C.; Wymer, C. *Inorg. Chem.* **2006**, *45*, 9558.

10.1021/ic7018204 CCC: $40.75
Published on Web 01/01/2008

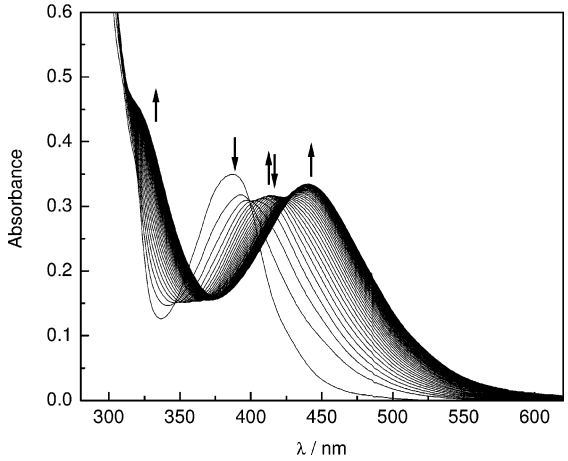

Figure 1. UV−vis spectra obtained upon irradiation of $[Ru(bpy)(AN)_4]^{2+}$ in water. Conditions $c_0 = 9.55 \times 10^{-5}$ M; $\lambda_{irr} = 390$ nm, $\Delta t = 90$ s.

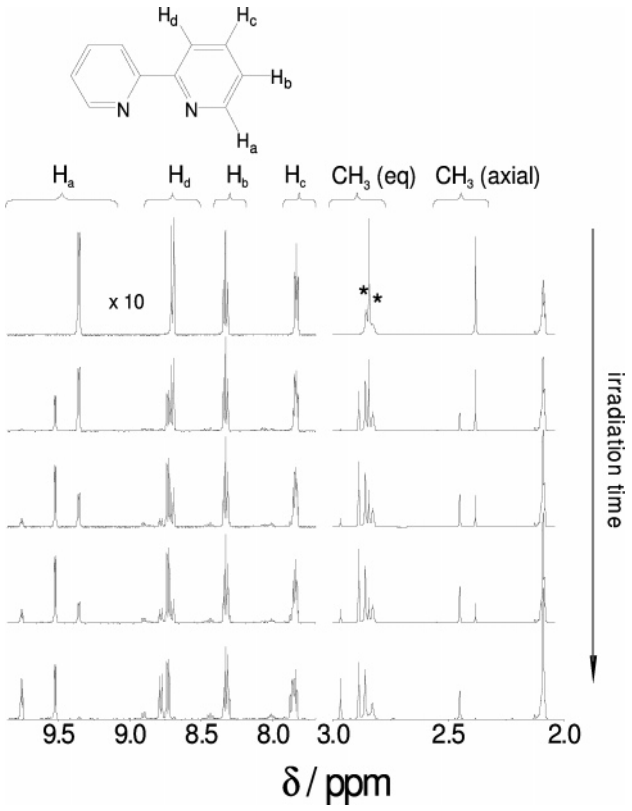

Figure 2. ^{1}H NMR spectra obtained during the photolysis of $[Ru(bpy)(AN)_4]^{2+}$ in acetone.

synthon to prepare heteroleptic polypyridine species by means of directed photocleavage of the axial acetonitrile molecules under mild visible-light irradiation conditions.

Materials and Methods

Physical Measurements. Microanalytical data for C, H, and N were obtained at INQUIMAE with a Carlo Erba EA 1108 analyzer. UV−vis spectra were recorded in acetone with a HP 8452A diode array spectrophotometer in a 1 cm path-length quartz cell. ^{1}H NMR spectra were recorded in acetone-d_6 using a Bruker AM-500 operating at 500 MHz. Fluorescence spectra were measured with a PTI Quantamaster spectrofluorometer. Visible light irradiation of

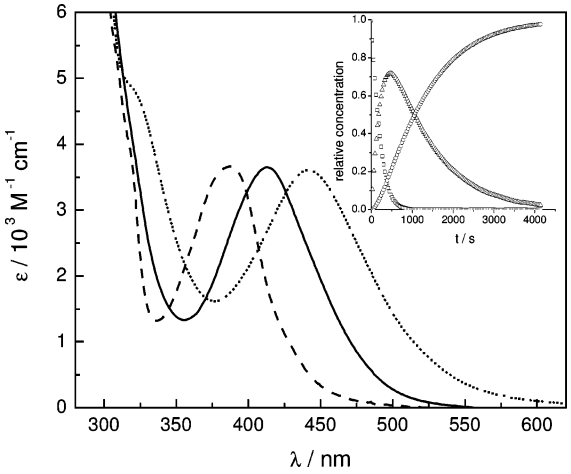

Figure 3. Deconvoluted spectra of the species involved in the photolysis experiment. Inset: calculated concentration profiles. See text for details.

samples during UV−vis measurements was performed using a 390 nm, 5 mm diameter light-emitting diode (LED). The light power of this source was calibrated in a test photolysis of *cis*-$[Ru(bpy)_2(py)_2]^{2+}$ (quantum yield of photosubstitution = 0.26).[1]

The photolysis experiments were also performed inside NMR tubes at higher concentration. In this case, a solution of $[Ru(bpy)(AN)_4](PF_6)_2$ in acetone-d_6 was irradiated using eight pulsed xenon lamps distributed around the NMR tube with the temperature kept at 10 °C by means of cold water circulation. A dye−gelatin filter was used to block all the wavelengths below 370 nm.

Syntheses. The reagents employed in this work were purchased from Aldrich or Merck and used without further purification. In all the synthetic procedures, the solutions were thoroughly degassed with N_2 prior to heating in order to prevent oxidation of the ruthenium aquo complexes. Compounds $Ru(bpy)Cl_4$ and $[Ru(bpy)(Py)_4](PF_6)_2$ were prepared according to literature procedures.[13]

$[Ru(bpy)(AN)_4](PF_6)_2$. A 540 mg (1.35 mmol) amount of $[Ru(bpy)Cl_4]$ and 240 mg (1.35 mmol) of ascorbic acid were dissolved in a mixture of 18 mL of water and 6 mL of acetonitrile and brought to 80 °C in the dark with constant stirring. The resulting deep yellow solution displayed an intense absorption at 388 nm at pH < 8. After 4 h, the UV−vis spectrum stabilized, indicating that the reaction attained completion. No changes in the absorption profile could be detected by alkalinization of an aliquot with NaOH, indicating the absence of aquo species. Precipitation was achieved with 2 equiv of solid KPF_6. The fine yellow powder was isolated by filtration, thoroughly washed with several portions of chilled water, and dried in vacuo. Yield = 700 mg (73%). Anal. Calcd: C, 30.39; H, 2.83; N, 11.81. Found: C, 30.6; H, 2.7; N, 11.9. NMR (acetone-d_6): ^{1}H δ 2.34 (s, 6H), 2.79 (s, 6H), 7.79 (t, 2H), 8.28 (t, 2H), 8.65 (d, 2H), 9.31 (d, 2H).

***trans*-$[Ru(bpy)(AN)_2(H_2O)_2]Cl_2$.** A 100 mg amount of $[Ru(bpy)(AN)_4](PF_6)_2$ (0.14 mmol) was dissolved in 10 mL of acetone and irradiated using a metal-halide lamp (Sylvania, HSI-TD CoralArc) through a 370 nm low-pass filter. The reaction was monitored by UV−vis until no changes were apparent. At this point the solution was treated with 5 mg of ascorbic acid and dissolved in 2 mL of water to eliminate a small amount of oxidation products. The solvent was removed under reduced pressure, and the resulting solid was redissolved in dry acetone and precipitated with a 1 M solution of TBA chloride in acetone. The reddish product was collected by

(13) Krause, R. A. *Inorg. Chim. Acta* **1977**, *22*, 209.

Scheme 1. Stepwise Conversion of $[Ru(bpy)(AN)_4]^{2+}$ into $[Ru(bpy)(AN)_3(H_2O)]^{2+}$ and $[Ru(bpy)(AN)_2(H_2O)_2]^{2+}$

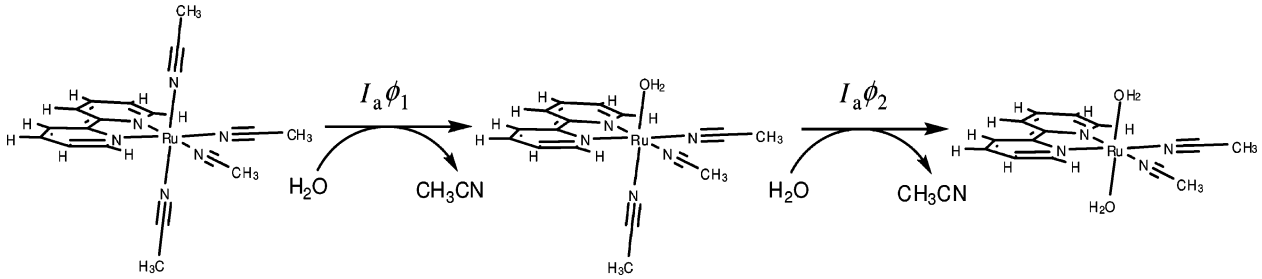

filtration, washed several times with acetone and dried in vacuo. Yield: 56 mg (90%). NMR (D_2O): ^1H δ 2.82 (s, 6H), 7.73 (t, 2H), 8.11 (t, 2H), 8.50 (d, 2H), 9.48 (d, 2H).

***trans*-[Ru(bpy)(AN)$_2$(PPh$_3$)$_2$](PF$_6$)$_2$.** To a solution of 30 mg of $[Ru(bpy)(AN)_2(H_2O)_2]Cl_2$ (0.067 mmol) in H_2O/MeOH (50:50) was added 44 mg (2.5 equiv) of triphenylphosphine (PPh_3), and it was allowed to react at 40 °C for 4 h in the dark with constant stirring. Once the reaction reached completion, the product was precipitated with 2 equiv of KPF_6 0.5 M, washed several times with water and dried over silica gel. Yield: 71 mg (92%). Anal. Calcd: C, 52.05; H, 3.84; N, 4.86. Found: C, 51.8; H, 3.9; N, 5.0. NMR (acetone-d_6): ^1H δ 2.58 (s, 6H), 7.12 (t, 2H), 7.24 (m, 12H), 7.33 (t, 12H), 7.43 (t, 6H), 7.88 (t, 2H), 8.11 (d, 2H), 8.38 (d, 2H).

Computational Methodology. We employed density functional theory (DFT) computations to fully optimize the ground-state geometries of the cationic species $[Ru(bpy)(AN)_4]^{2+}$, *fac*-$[Ru(bpy)(AN)_3(H_2O)]^{2+}$, and *trans*-$[Ru(bpy)(AN)_2(H_2O)_2]^{2+}$ in vacuo, without symmetry constraints. The calculations were performed with Gaussian 03[14] at the B3LYP level[15] employing the effective core potential basis set LanL2DZ basis, which proved to be suitable for geometry predictions in coordination compounds containing metals of the second row of the transition elements in the Periodic Table. We used tight SCF convergence criteria and default settings in the geometry optimizations. The true nature of the stationary points was explored by numerical vibrational frequency computations. The absence of negative frequencies confirmed that the optimized geometries correspond to stable configurations in the ground-state potential-energy surface.

In the analysis of the electronic structure, including spectral calculation and assignment, we included the solvent treated as a continuum dielectric medium using the PCM approximation, as implemented in Gaussian 03.

(TD)DFT was employed to compute the excited-state energies and compositions. The energies and intensities of the lowest 100 singlet−singlet and singlet−triplet electronic transitions were calculated with (TD)DFT which covered the region up to 200 nm.

The geometry of the lowest energy triplet state of $[Ru(bpy)(AN)_4]^{2+}$ was also obtained by DFT. Unrestricted open-shell calculations with the same basis sets were performed in this case. The ^{3}MLCT excited state (see later) was optimized using the ground-state geometry as an initial guess. A full scan of the Ru−N(ax) bond length followed by a full optimization allowed us to locate a second minimum which corresponds to the ^{3}d−d excited state. In both cases, frequency calculations were performed to establish the nature of the critical points (minimum or transition state).

(14) *Gaussian 03*, revision D.01; Gaussian, Inc.: Wallingford, CT, 2004.
(15) Becke, A. D. *J. Chem. Phys*. **1993**, *98*, 5648.

Results and Discussion

When aqueous solutions of $[Ru(bpy)(AN)_4]Cl_2$ are irradiated with 390 nm light, the electronic spectrum changes as shown in Figure 1.

The first few spectra share an isosbestic point at 399 nm, which rapidly disappears, suggesting that the primary photoproduct, which forms in the first few minutes of irradiation and has an absorption maximum that is red shifted if compared to $[Ru(bpy)(AN)_4]^{2+}$, is also photoreactive. The intermediate solutions obtained during the photolysis experiment remain unchanged if the illumination is removed, indicating that all the species present in solution are thermally stable. After prolonged illumination, the spectral changes slow down, leading to the final product that shows an absorption maximum at ca. 450 nm. When the spectra are analyzed by factor analysis[16,17] only three colored species can be detected. Altogether, this information suggests a two-step photomechanism where acetonitrile molecules in the coordination sphere are consecutively displaced by an increasing number of better σ-donor water molecules, leading to $[Ru(bpy)(AN)_3(H_2O)]^{2+}$ and $[Ru(bpy)(AN)_2(H_2O)_2]^{2+}$. Notice that the UV−vis experiment does not rule out the possibility of parallel reactions yielding the different isomers of the mono-aquo and bis-aquo species (two and three, respectively).

In order to gain extra information on the reaction, we also performed the photolysis inside an NMR tube. In this case, because of solubility reasons we chose to work in acetone-d_6 in the presence of a small amount of water. Figure 2 depicts the NMR spectra at different irradiation times. Analysis of the spectra reveals that (a) the six signals of $[Ru(bpy)(AN)_4]^{2+}$ disappear steadily, (b) a second species with six distinguishable protons grows in the first few seconds but slowly disappears, (c) a third species that has the same number of signals grows steadily, and (d) the concentration of free acetonitrile increases with time (its signal appears overlapped with the solvent residual signal at $\delta = 2.09$ ppm). (e) The three species have only four signals in the aromatic region, suggesting that both pyridine rings are equivalent. (f) The intermediate species shows signals in the aliphatic region at 2.89 and 2.45 ppm in a 1:2 ratio, but the final product has only one type of methyl protons. Altogether, these results lead to the conclusion that the photodissociation steps occur solely on the axial positions as in Scheme 1.

(16) Malinovsky, E. R. *Factor Analysis in Chemistry*, 2nd ed.; Wiley-Interscience: New York, 1991.
(17) Slep, L. D.; Pollak, S.; Olabe, J. A. *Inorg. Chem*. **1999**, *38*, 4369.

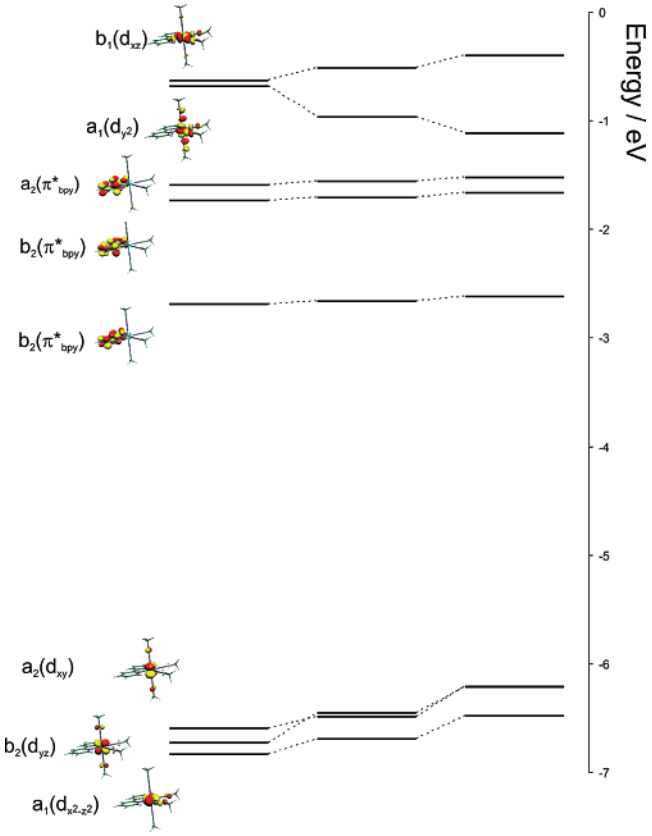

Figure 4. Frontier molecular orbital diagram for (from left to right) $[Ru(bpy)(AN)_4]^{2+}$, *trans*-$[Ru(bpy)(AN)_3(H_2O)]^{2+}$, and *trans*-$[Ru(bpy)(AN)_2(H_2O)_2]^{2+}$. The symmetry labels correspond to $[Ru(bpy)(AN)_4]^{2+}$ analyzed under the C_{2v} point group. See text for details.

A global analysis of the experimental spectra according to this model renders the quantum yields for the consecutive photodissociation steps (0.43 and 0.09, respectively) and the spectra displayed in Figure 3 for the three species $[Ru(bpy)(AN)_4]^{2+}$, *fac*-$[Ru(bpy)(AN)_3(H_2O)]^{2+}$, and *trans*-$[Ru(bpy)(AN)_2(H_2O)_2]^{2+}$. The very high quantum yield for the first step is not unexpected provided the experimental correlation described for the related $Ru(bpy)_2XY$ complexes between the photoaquation quantum yield and the energy of the MLCT band.[1] Substitution of the axial acetonitrile leads to significant shifts in the lowest energy absorption maximum to 413 and 442 nm for the mono- and bis-aquo species, respectively.

Analysis of the Stereoselectivity upon Irradiation. It is a well-known fact that ruthenium polypyridine compounds can undergo photodissociation following irradiation. The photochemistry of the $[Ru^{II}(bpy)_2L_2]^{n+}$ species, usually involving release of one of the monodentate L ligands, has been classically rationalized as arising from a dissociative ^3d-d state, which can be thermally populated after irradiation of the lowest energy MLCT absorption band.[1] With this scheme in mind we started by exploring the electronic states of $[Ru(bpy)(AN)_4]^{2+}$ using DFT and (TD)DFT.

The geometry of $[Ru(bpy)(AN)_4]^{2+}$ (as a $CF_3SO_3^-$ salt) has been recently examined by X-ray diffraction.[18] The Ru(II) ion is in a close to octahedral N_6 environment with average Ru−N(bpy), Ru−$N(AN_{eq})$, and Ru−$N(AN_{ax})$ bond lengths of 2.047, 2.045, and 2.026 Å, respectively. The DFT computations nicely reproduce these features: Ru−N(bpy), Ru−$N(AN_{eq})$, and Ru−$N(AN_{ax})$ bond lengths of 2.07, 2.09, and 2.05 Å (the calculated distances being slightly longer than the experimental ones, as already observed for other complexes when performing DFT-ECP (effective core potential) calculations)[19,20] and $N(AN_{eq})$−Ru $N(AN_{eq})$, $N(AN_{eq})$−Ru−N(bpy), and N(bpy)−Ru−N(bpy) angles of 86.5°, 97.1°, and 79.3°. The bpy ligand and equatorial AN molecules lay on the same plane as the metal center. The other two solvent molecules occupy the axial positions, colinear with the *y* axis and strictly perpendicular to the equatorial *xz* plane that contains the bpy moiety. This plane constitutes one symmetry element of the molecule as does a second plane perpendicular to this one. The latter *yz* plane contains the metallic center and roughly bisects the bipyridine molecule.

Replacement of an axial acetonitrile by a water molecule renders *fac*-$[Ru(bpy)(AN)_3(H_2O)]^{2+}$. This species shows a ligand environment that except for the exchange of AN by H_2O preserves the fundamental characteristics: Ru−N(bpy), Ru−$N(AN_{eq})$, Ru−$N(AN_{ax})$, and Ru−O bond lengths of 2.07, 2.05, 2.01, and 2.17 Å, respectively. Substitution of a second axial molecule leads to *trans*-$[Ru(bpy)(AN)_2(H_2O)_2]^{2+}$ with Ru−N(bpy), Ru−$N(AN_{eq})$, and Ru−O bond lengths of 2.07, 2.09, and 2.14 Å.

As shown above, deviations from an idealized C_{2v} geometry in $[Ru(bpy)(AN)_4]^{2+}$ are small, and this point group can be safely assumed in any qualitative analysis of the electronic structure of this species. Replacement of one axial ligand lowers the symmetry to C_s, but the C_{2v} description is recovered for $[Ru(bpy)(AN)_2(H_2O)_2]^{2+}$. Figure 4 represents the relevant computed MO's in the three related species.

We start the analysis with the original tetrakis acetonitrile molecule. Under C_{2v} symmetry, the octahedral $d_\pi(t_{2g})$ set splits into $a_1(d_{x^2-z^2})$, $b_2(d_{yz})$, and $a_2(d_{xy})$. The degeneracy of the $d_\sigma(e_g)$ set is also lifted with the individual orbitals transforming as $a_1(d_{y^2})$ and $b_1(d_{xz})$. The DFT calculations suggest that the t_{2g} orbitals remain mostly metal-centered with at least 70% Ru orbital character and the remaining contributions arising mostly from filled π orbitals of the ligands. The HOMO is comprised mostly by the Ru $a_2(d_{xy})$ orbital, while HOMO-1 and HOMO-2 can be assigned to the b_2 and a_1 metal orbitals. The Ru−bpy back-bonding is rather small and manifests in the composition of the LUMO, which is mostly a b_2 bpy-centered orbital with a marginal (3.5%) $Ru(d_{yz})$ contribution. The remaining vacant metal-centered e_g orbitals are involved in the antibonding LUMO+3 and LUMO+4 and span the a_1 and b_1 irreducible representations, respectively. The electronic structure calculations are overall consistent with a small degree of metal−

(18) Lackner, W.; Standfest-Hauser, C. M.; Mereiter, K.; Schmid, R.; Kirchner, K. *Inorg. Chim. Acta* **2004**, *357*, 2721.

(19) Li, J.; Noodleman, L.; Case, D. A. Electronic Structure Calculations with Applications to Transition Metal Complexes. In *Inorganic Electronic Structure and Spectroscopy*; Solomon, E. I., Lever, A. B. P., Eds.; Wiley: New York, 1999; Vol. I, pp 661−724.

(20) Videla, M.; Jacinto, J. S.; Baggio, R.; Garland, M. T.; Singh, P.; Kaim, W.; Slep, L. D.; Olabe, J. A. *Inorg. Chem.* **2006**, *45*, 8608.

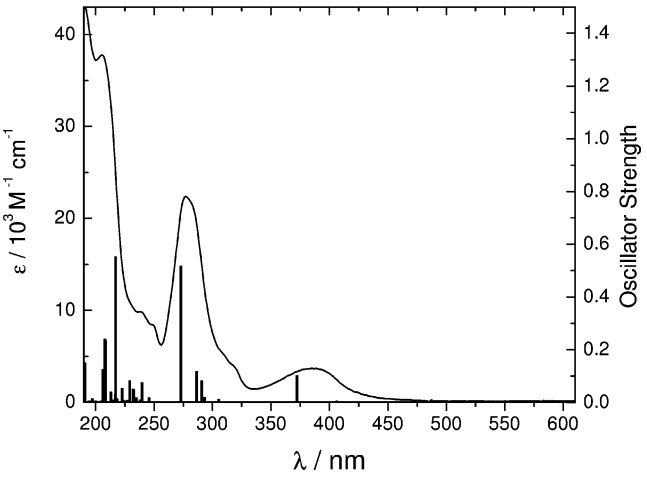

Figure 5. Electronic spectrum of $[Ru(bpy)(AN)_4]^{2+}$ in water. The vertical lines are the (TD)DFT computed transitions. See text for details.

ligand covalency (Ru−N Mayer bond orders of 0.43, 0.31, and 0.27 for the Ru−N(bpy), Ru−N(AN_{ax}), and Ru−N(AN_{eq}) bonds).

The picture remains similar upon consecutive replacement of the axial acetonitrile fragments. The main changes are the progressive shift of the d_π orbitals to higher energy and most noticeably an increasing splitting of the e_g set.

The electronic spectrum of $[Ru(bpy)(AN)_4]^{2+}$ in Figure 5 shows several intense transitions that are roughly solvent independent. In aqueous solutions the absorption maxima are located at 272 ($\epsilon = 77.9 \times 10^3$ M^{-1} cm^{-1}) and 384 nm ($\epsilon = 5.0 \times 10^3$ M^{-1} cm^{-1}). The (TD)DFT computations are in good agreement with the experimental spectra and allow for a full assignment of the electronic transitions. The lowest energy band at 384 nm (computed at 372 nm, $f = 0.098$) arises from the *z*-polarized HOMO-1 → LUMO ($b_2(d_{yz})$ → $b_2(\pi^*_{bpy})$ CT transition. The contribution of the HOMO → LUMO $a_2(d_{xy})$ → $b_2(\pi^*_{bpy})$ to this absorption is negligible, even when symmetry allowed, because of the very poor overlap between the metal and ligand orbitals. A second *z*-polarized CT absorption, which has mixed $b_2(d_{yz})$ → $b_2(\pi^*_{bpy})$ (HOMO-1 → LUMO+1) and $a_2(d_{xy})$ → $a_2(\pi^*_{bpy})$ (HOMO → LUMO+2) character is predicted at 286 nm ($f = 0.113$). The intraligand $\pi \rightarrow \pi^*$ transition is expected at 273 nm. These two overlapping transitions account for the strong absorption at 272 nm ($f = 0.512$).

The UV−vis spectra of the mono- and di-aquo species obtained by photolysis still show an intense absorption in the visible range shifted to lower energies (maxima at 413 and 442 nm, respectively). The (TD)DFT computations are consistent with these findings, positioning the lower energy MLCT at 404 ($f = 0.092$) and 424 nm ($f = 0.106$), respectively, in agreement with the experimental results.

The lowest energy ^{3}MLCT excited-state optimized geometry and spin density of $[Ru(bpy)(AN)_4]^{2+}$ is represented in Figure 6a. Even when the lowest energy absorption spin allowed MLCT band in $[Ru(bpy)(AN)_4]^{2+}$ can be ascribed to the HOMO-1 → LUMO ($b_2(d_{yz})$ → $b_2(\pi^*_{bpy})$ CT transition, the associated triplet state is actually more unstable (ca. 2000 cm^{-1}) than the one with $a_2(d_{xy})$ → $b_2(\pi^*_{bpy})$ character. The

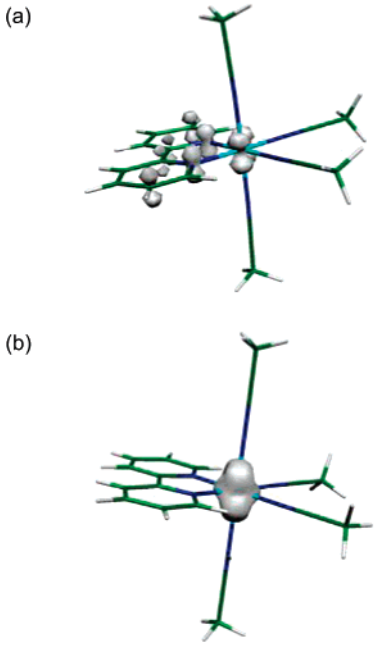

Figure 6. Geometry and spin density of the DFT-optimized lowest energy (a) ^{3}MLCT and (b) ^{3}d−d excited states of $[Ru(bpy)(AN)_4]^{2+}$.

optimized geometry of this excited state reveals Ru−N(bpy), Ru−N(AN_{eq}), and Ru−N(AN_{ax}) bond lengths of 2.02, 2.13, and 2.05 Å, respectively.

Immediately above the two ^{3}MLCT states it is possible to find the first ^{3}d−d excited state. This state is $a_2(d_{xy})$ → $a_1(d_{y^2})$ in character and lays only 3000 cm^{-1} above the $a_2(d_{xy})$ → $b_2(\pi^*_{bpy})$ ^{3}MLCT and ca. 1000 cm^{-1} below a second ^{3}d−d state that is $a1(d_{x^2-z^2})$ → $b_1(d_{xz})$ in character. When allowed to relax, the lower energy ^{3}d−d state has much longer Ru−N(AN_{ax}) bond lengths but comparable Ru−N(AN_{eq}) ones (2.54 and 2.13 Å, respectively). This is not unexpected provided that the $a_1(d_{y^2})$ orbital is antibonding particularly with respect to the axial ligands. Notice that this particular ordering is a consequence of the stronger σ-donor ability of the bpy fragment compared to the rest of the coordination sphere. Figure 6b shows the optimized geometry and spin density of this state. This findings suggest the following pathway for the photochemistry of $[Ru(bpy)(AN)_4]^{2+}$ that justifies the observed photoreactivity. (1) Population of the ^{1}MLCT HOMO-1 → LUMO ($b_2(d_{yz})$ → $b_2(\pi^*_{bpy})$ state. (2) Intersystem crossing that leads to population of the ^{3}MLCT $a_2(d_{xy})$ → $b_2(\pi^*_{bpy})$ state. (3) Thermal population of the ^{3}d−d $a_2(d_{xy})$ → $a_1(d_{y^2})$ state with elongated bonds in the axial axis. (4) Substitution of one axial acetonitrile.

It is not difficult to realize that compounds that result from modifications of the first coordination sphere without introducing stronger σ-donor ligands than bpy should behave in a very similar way. On the contrary, substitution by moderately strong Lewis bases can yield very different results. For instance, solutions of $[Ru(bpy)(py)_4]^{2+}$ undergo spectral changes when irradiated on the visible-range MLCT band. However, NMR analysis shows no apparent selectivity. The photodissociation of any of the four pyridines in the

compound appears as roughly equiprobable, yielding complex mixtures of isomers that cannot be easily resolved.

Synthetic Applications. The photolysis procedure is scalable for synthetic purposes. Given the high quantum yield of the photoreaction, tens to hundreds of milligrams of $[Ru(bpy)(AN)_4]^{2+}$ can be photolyzed in a few hours using a normal 150 W metal-halide lamp. In water, alcohols, or acetone, photolysis of soluble salts of the complex yields only *trans*-$[Ru(bpy)(AN)_2(solv)]^{2+}$, which can be used directly for further reactions or be isolated as a chloride salt by precipitation with tetrabutylammonium chloride in dry acetone.

The photolyzed species, bearing two *trans*-labile ligands, can be easily used as a *trans* core for making heteroleptic complexes having just one bipyridine. As previously stated, if the product has weak donor ligands, it keeps the photochemical properties of the tetrakis acetonitrile complex. The triphenylphosphine complex *trans*-$[Ru(bpy)(AN)_2(PPh_3)_2](PF_6)_2$ is a good example, yielding *trans*-$[Ru(bpy)(AN)_2(PPh_3)(H_2O)](PF_6)_2$ and *trans*-$[Ru(bpy)(AN)_2(H_2O)_2](PF_6)_2$ as unique photoproducts upon irradiation in water, acetone, or alcohols. The bis-PPh_3 product was not obtained by thermal substitution in the dark.

Conclusions

We have shown that the complex $[Ru(bpy)(AN)_4]^{2+}$ undergoes a very clean photoreaction yielding only *trans*-$[Ru(bpy)(AN)_2(solv)_2]^{2+}$ when irradiated with visible light in an adequate solvent. The obtained species, bearing two labile axial ends, can be used as a core for synthesis of other *trans* complexes. Complexes of the form *trans*-$[Ru(bpy)(AN)_2L_2]^{2+}$, L being a poorly basic ligand such as PPh_3, thioethers, or other nitriles, retain the photochemical properties and also photodeliver the axial ligands L without decomposition on the equatorial plane.

Acknowledgment. This research was supported by the National Agency for Science and Technology Promotion (ANPCyT 14013), University of Buenos Aires (UBACyT X037), and CONICET. R.E. and L.D.S. are members of the research staff of CONICET.

IC7018204